The Solar Wind Electron Halo as Produced by Electron Beams Originating in the Lower Corona: Beam Density Dependence

H. Che (University of Alabama in Huntsville)
M. L Goldstein (Space Science Institute, Boulder, CO)
C. S. Salem (Space Science Institute, University of California, Berkeley, CA)
A. F. Vinas (Nasa Goddard Flight Center, Greenbelt, MD)

The Origin of Electron Halo of Solar Wind Is A Puzzle

Pilipp et al, 1987, JGR

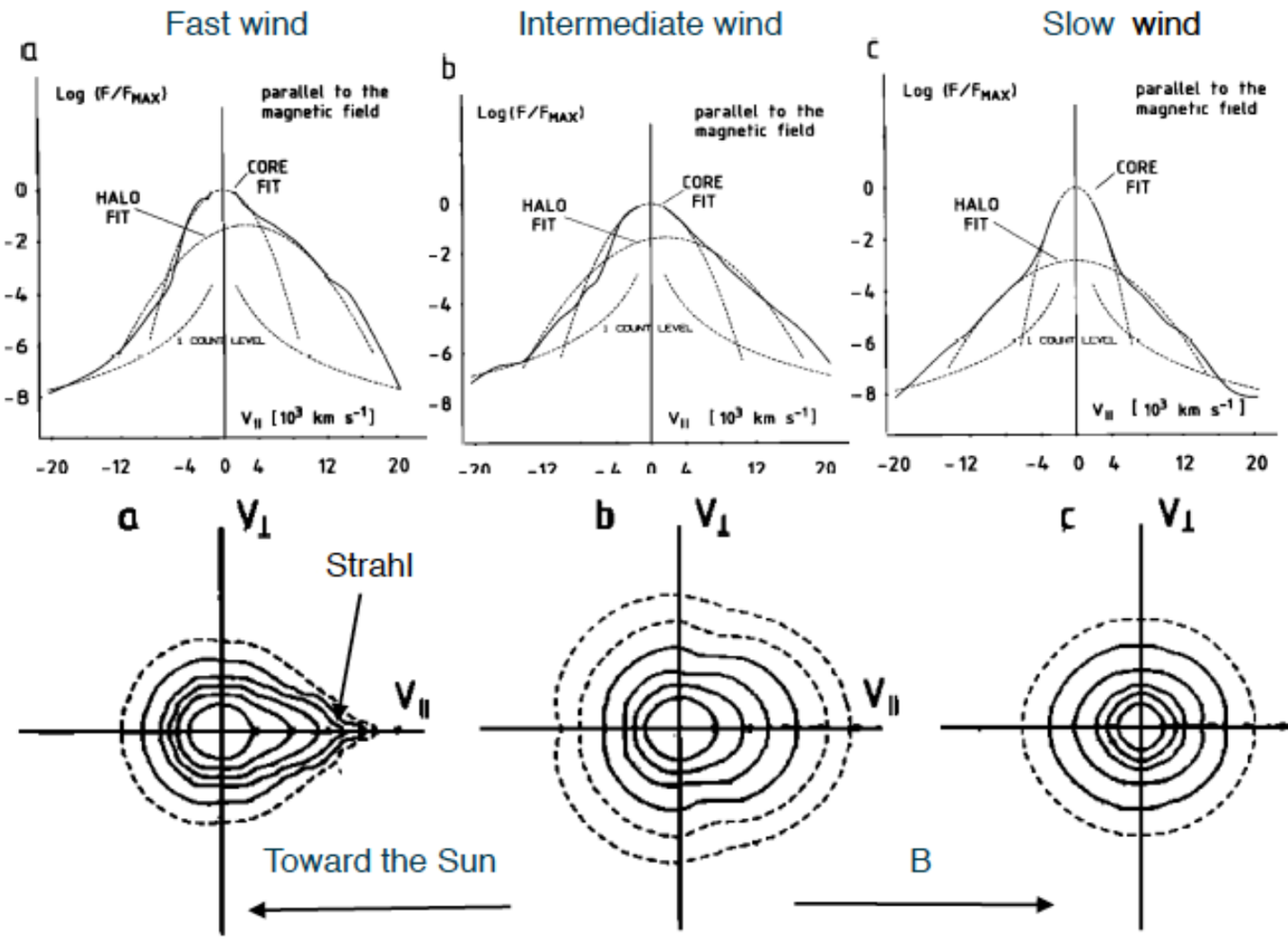

Helios observations show electron Halo already forms at 0.3 AU and propagates to 1AU.

Numerous studies show that the formation of halo requires strong wave scattering generated by kinetic instabilities (Marsch, LRSP,2006)

Vocks et al (2005) argue that halo may be developed by whistler wave in the solar corona.

Ko et al. 1996 ;Esser & Edgar 2000; Laming 2004; Feldman et al. 2008 discovered that the electron velocity distribution function in the lower corona have a superathermal tail.

Strahl in the fast wind is believed to be formed by magnetic focusing effects.

The Origin of Electron Beams and Solar Flares

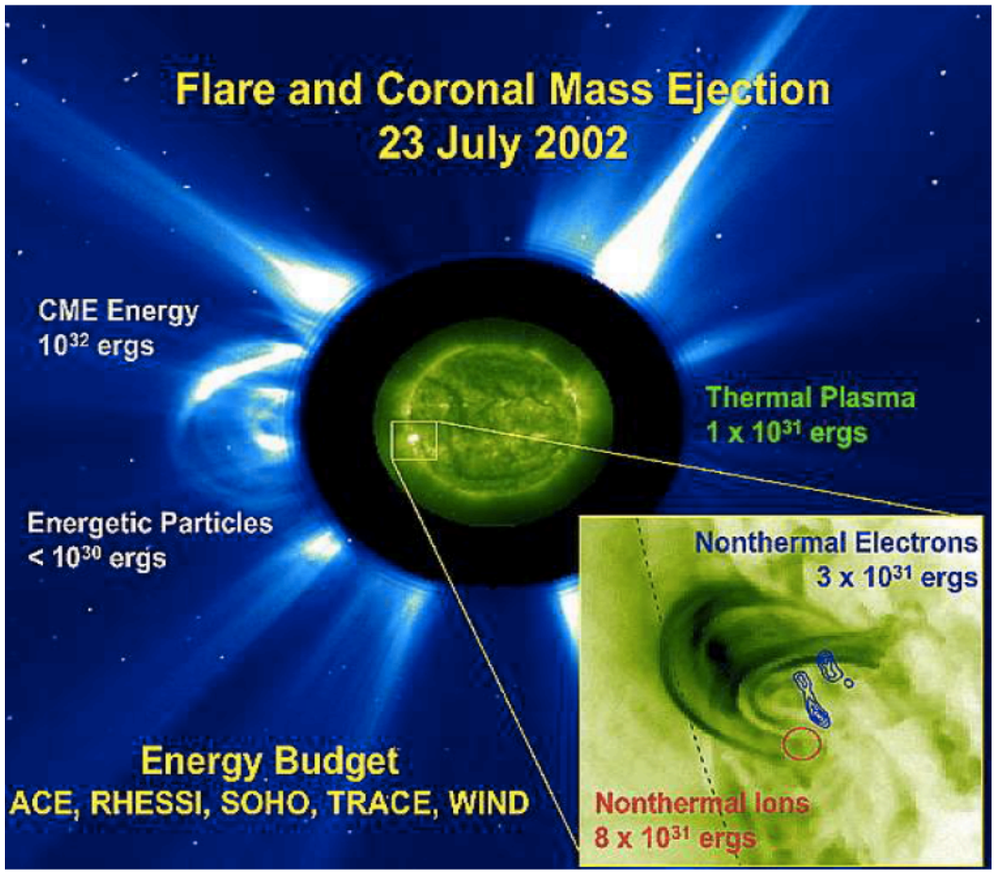

Emslie et al, 2004, 2005

Benz, 2017

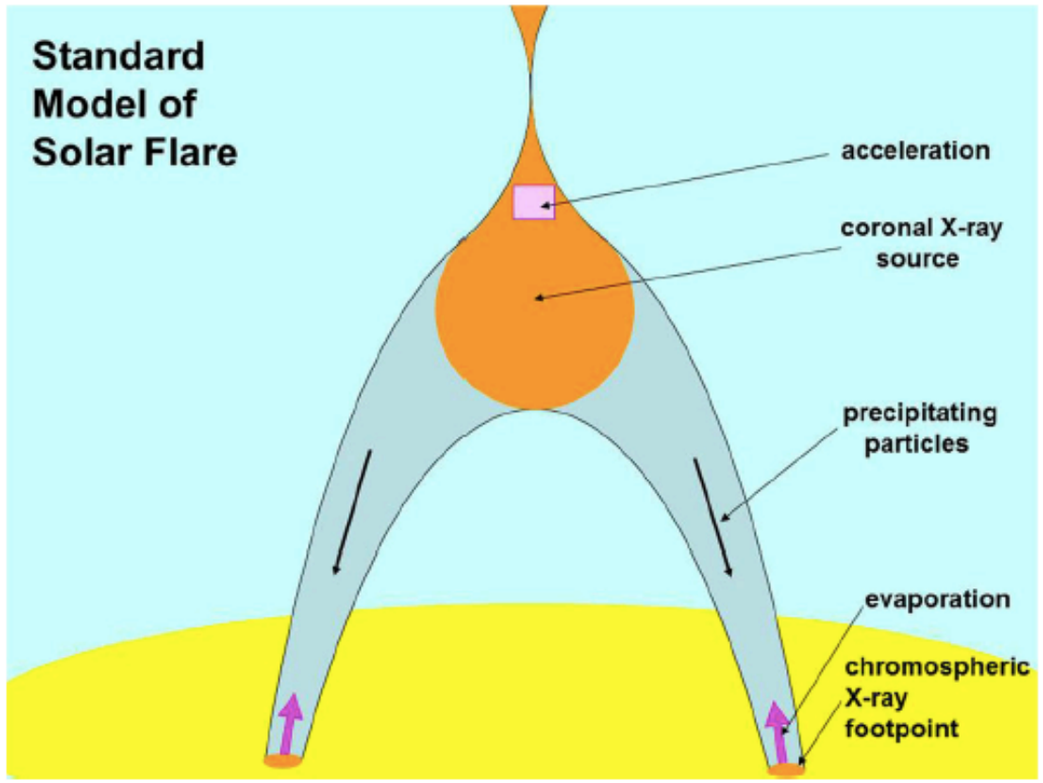

Fig. 13 A schematic drawing of the standard flare scenario assuming energy release at high altitudes

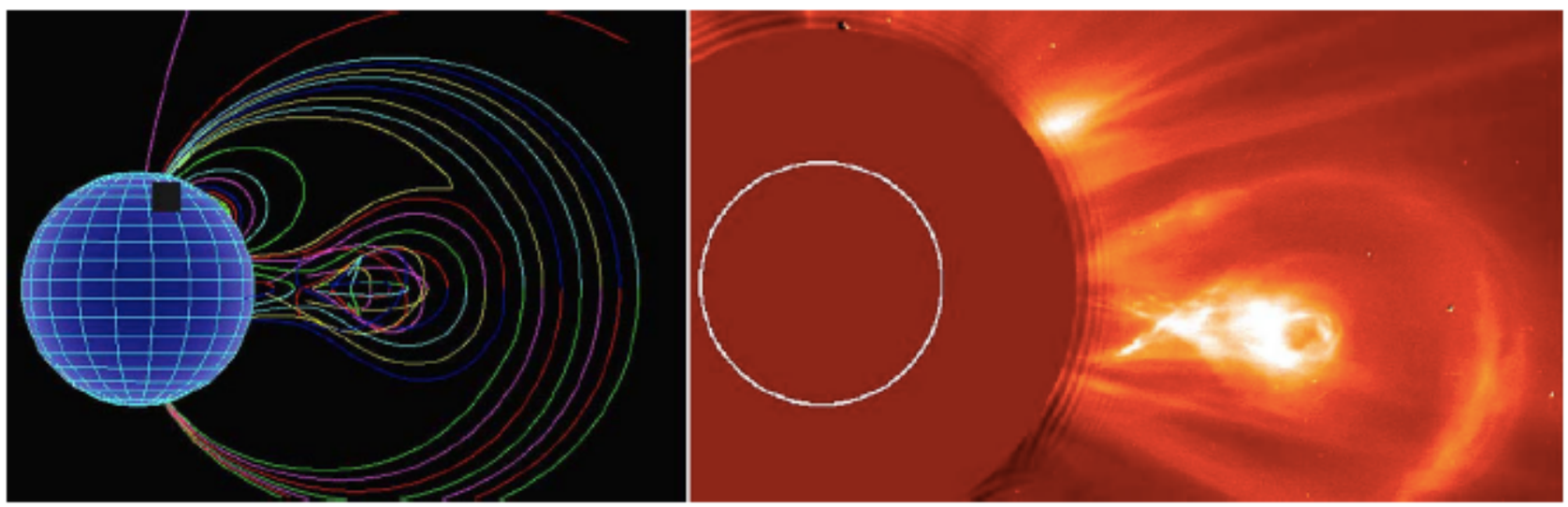

Fig. 16 *Left* a schematic drawing of the one-loop flare model. *Right* observation of an apparent X-point behind a coronal mass ejection observed by LASCO/SOHO in white light (copyright by NASA)

Evidence of Nanoflare-associated Electron beams

Electron beams accelerated during nanoflares produce weak coronal Type III radio bursts with Tb~10^7 K~keV. The keV electron beams — Free energy.

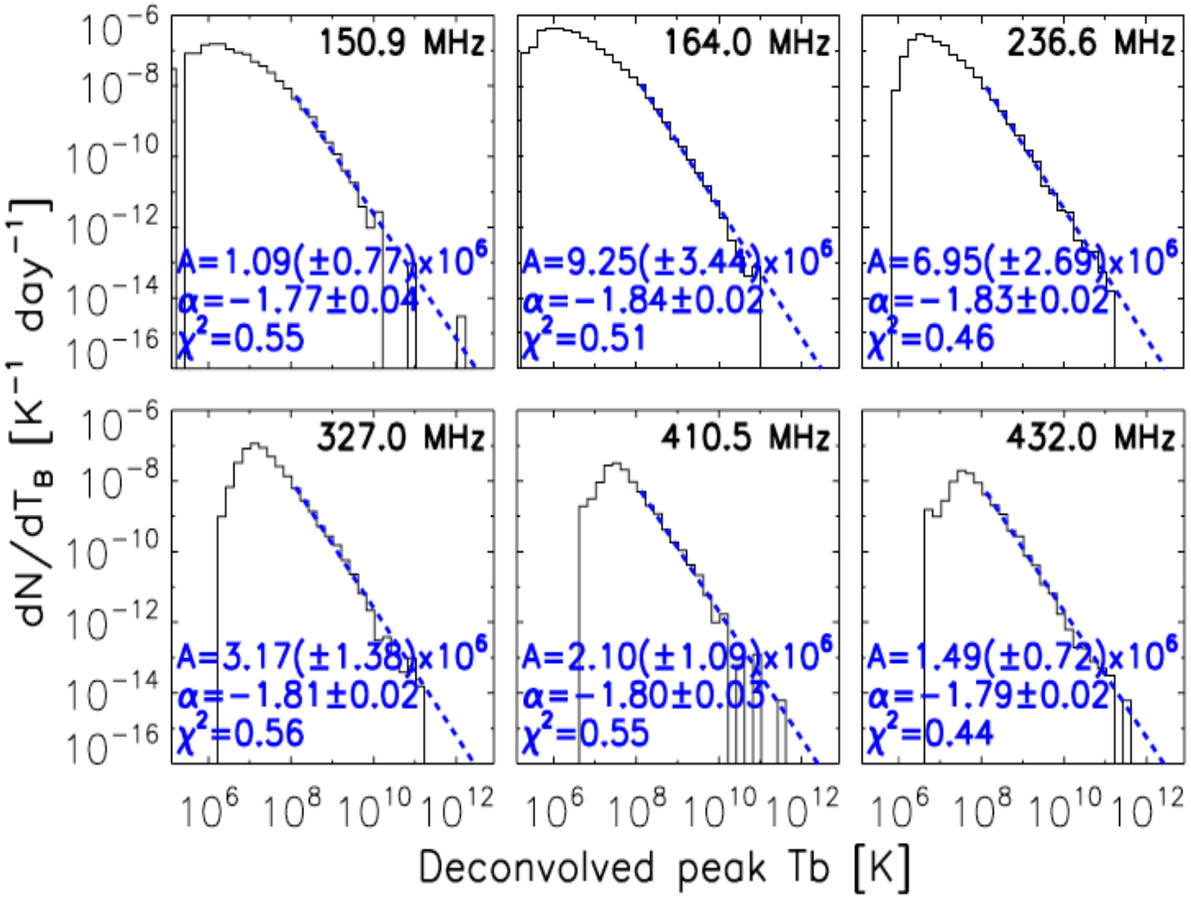

The typical Tb for flare type III radio bursts is ~10^15 K

Statistical survey 10,000 type III radio bursts observed by the Nancy Radioheliograph from 1998 to 2008 found associated with nanoflares (Saint-Hilaire et al, ApJ, 2013).

Nanoflares

(proposed by E. Parker in 1988. Recent Hi-C, SDO and IRIS provide both direct and indirect evidences for the existence)

	Solar Flare	Nanoflare
Energy	10^{32} ergs	10^{23} -10^{24} ergs ~10^{-9} flare
Location and Size	Active region (10^{6} km)	Everywhere (1000 km)
Occurrence Rate	Several a day at active-time and less than one per week at quite-time.	10^{6} nanoflares per second in the whole Sun, even at the Sun quiet-time.
Electron Density Ratio	25-50% of background	~should not be small

Nanoflares may provide semi-continuous free energy.

The Connection Between Nanoflares and Solar Wind

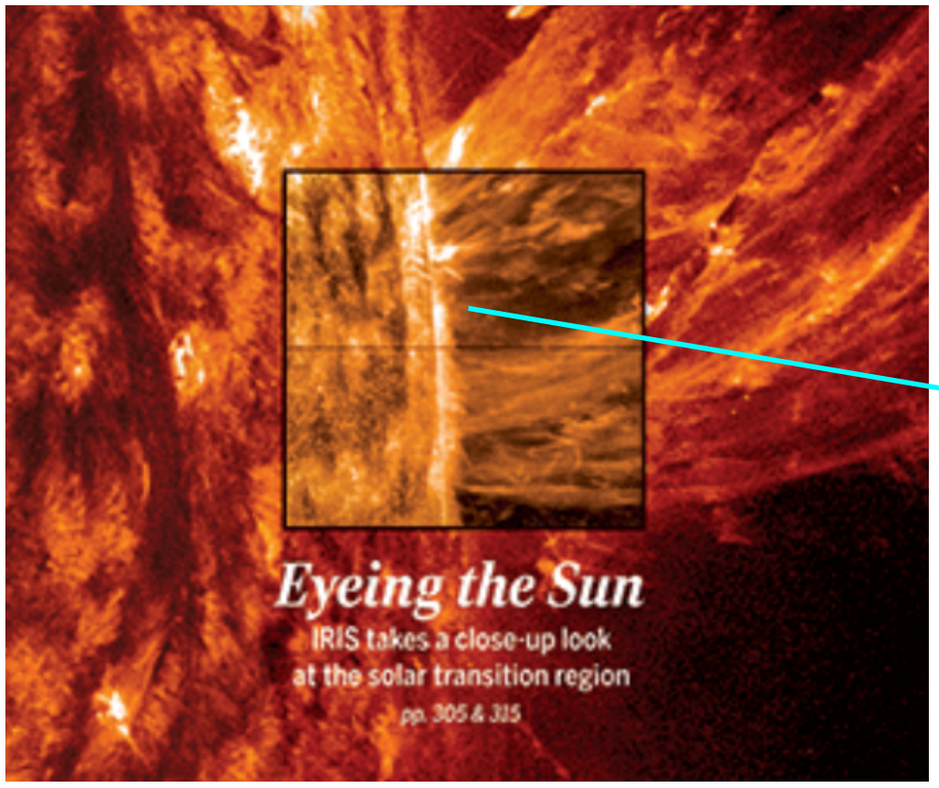

IRIS science special issue, 2005

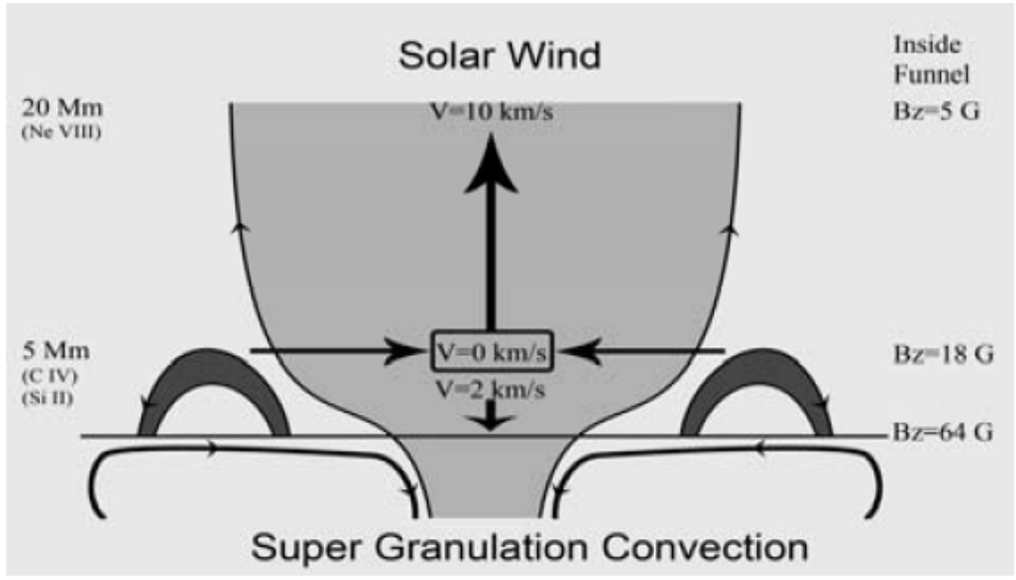

Marsch, ILWS workshop 2006

Nanoflares: merging of small magnetic loops rooted from photosphere due to the super granulation convection.
Solar Wind: originating from the plasma ejected by Nanoflares.

Evidence of Nanoflare-Origin Solar Wind

Fast Wind>400km/s

- Nearly Photospheric composition
- Frozen-in temperature 8x10^5
- From coronal hole

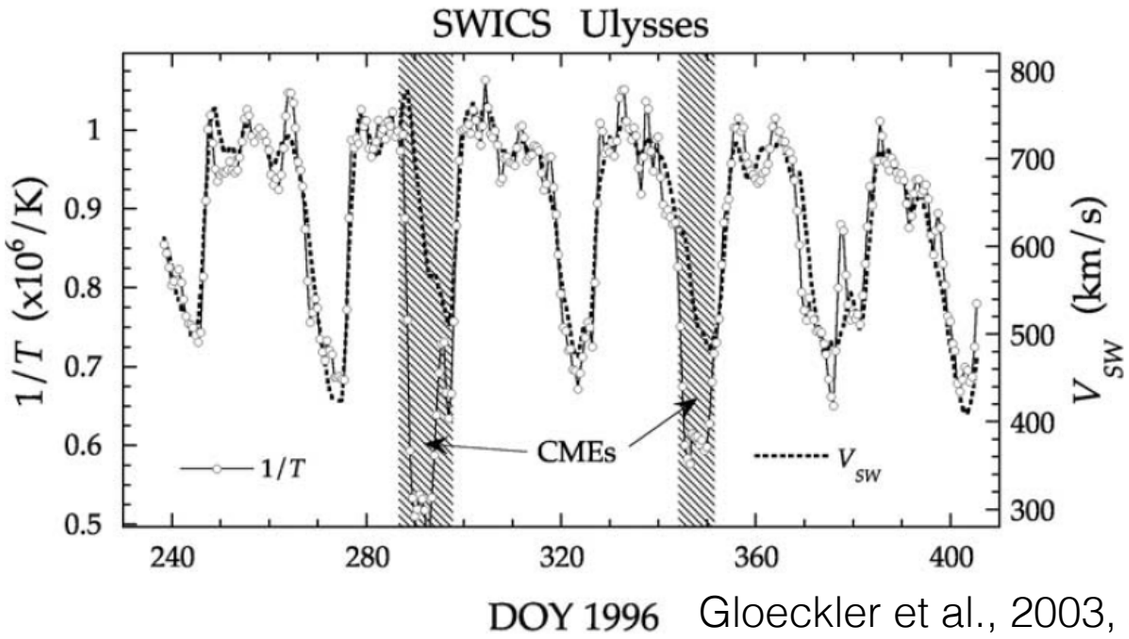

Gloeckler et al., 2003, JGR

Slow Wind <400km/s

- Lower Coronal composition
- Frozen-in temperature 1.5x10^6
- From quiet Sun

Feldman et al., 2005, JGR

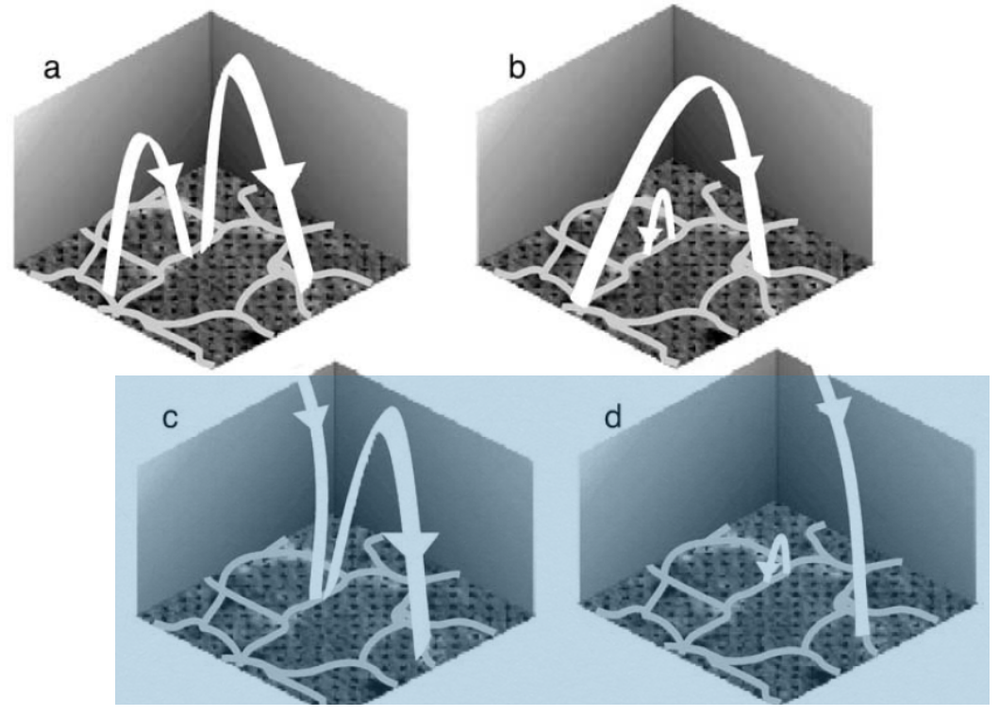

Fisk Kinetic Solar Wind Model, 2003, JGR

Generation of KAW and Whistler waves by Weibel Instability and Inverse Energy Cascade

Che, Goldstein, and Vinas, PRL, 2014

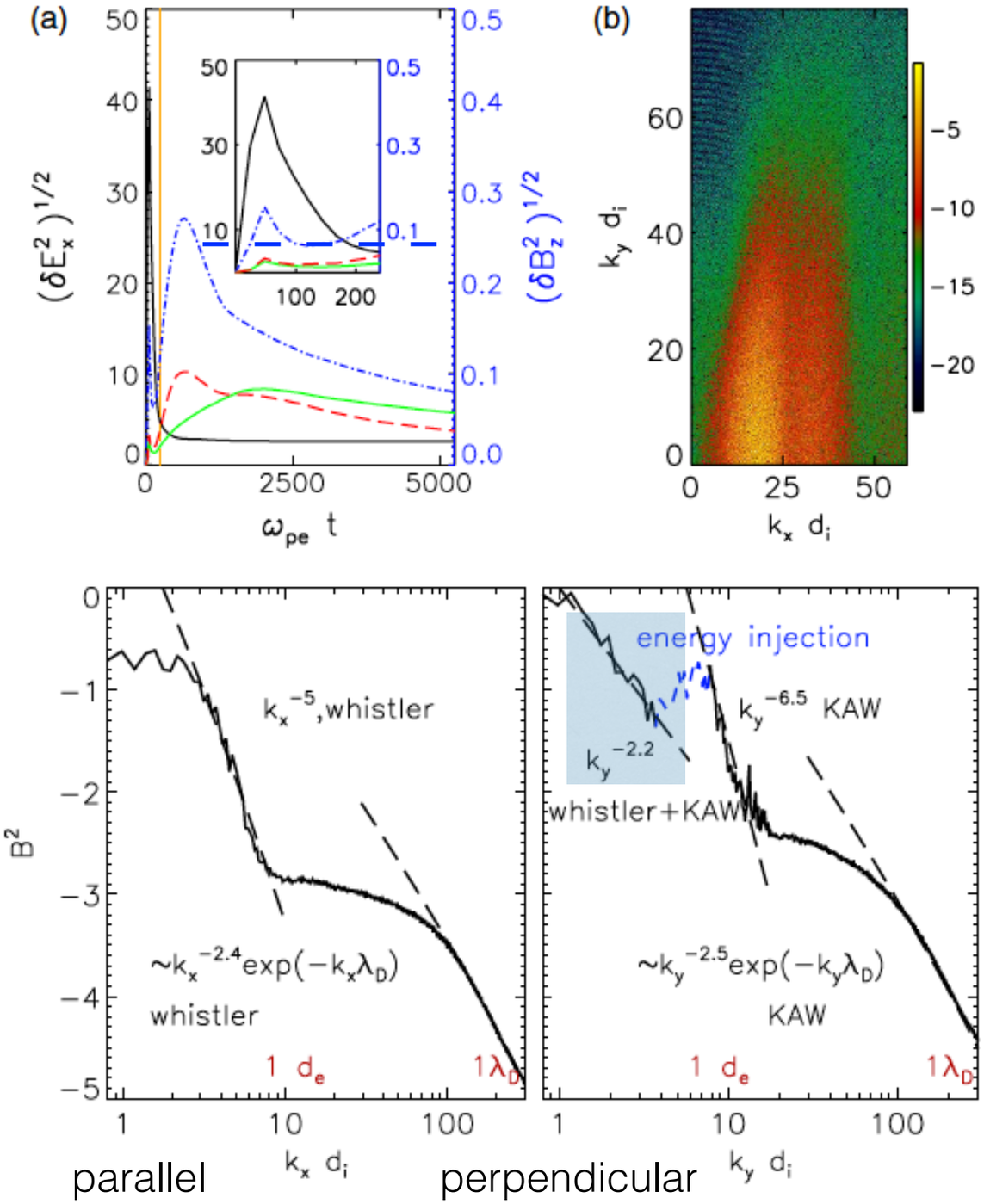

magnitude of &B is ~20% of background

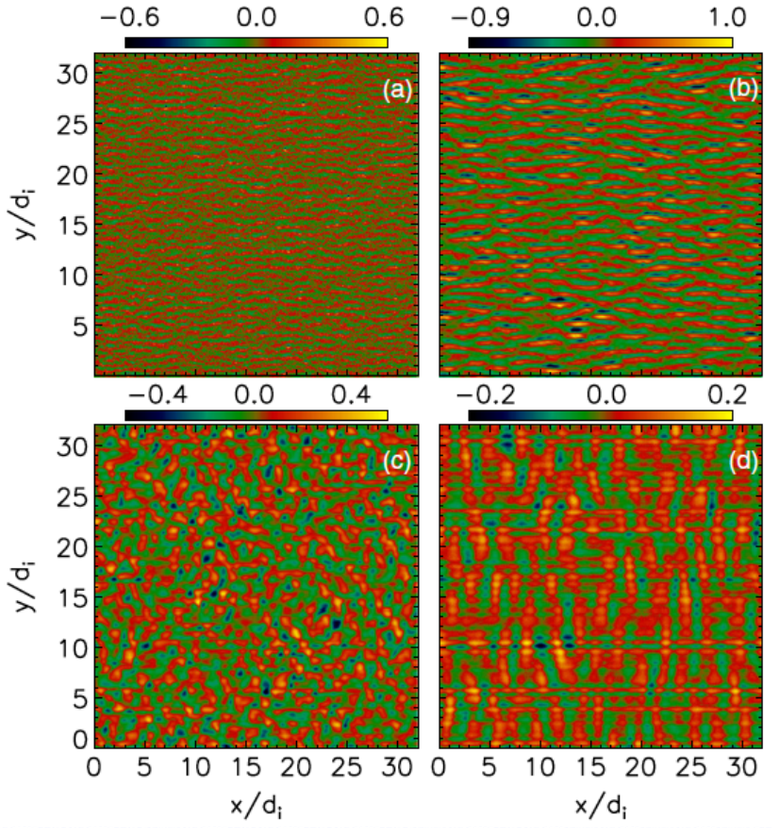

Observation of solar wind KAW

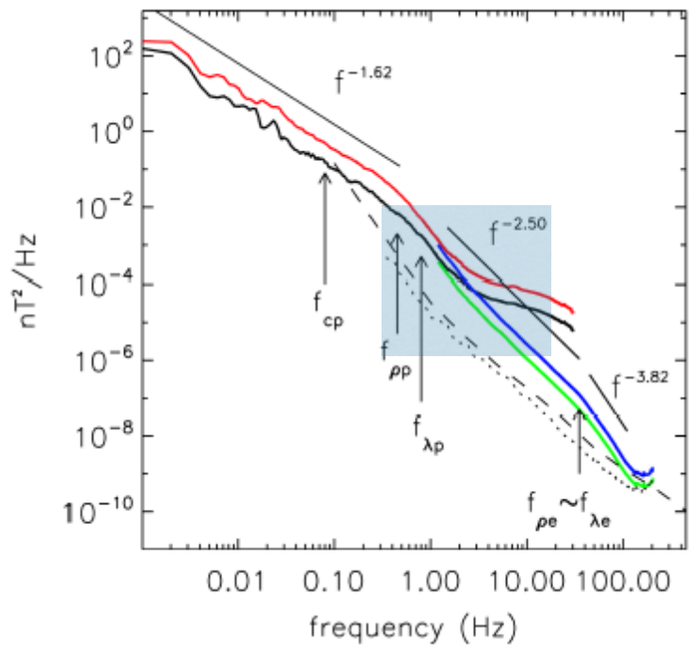

Sahraoui, et al, 2009, PRL

Formation of Electron Halo in the Solar Wind

Che & Goldstein, ApjL, 2014

Simulation

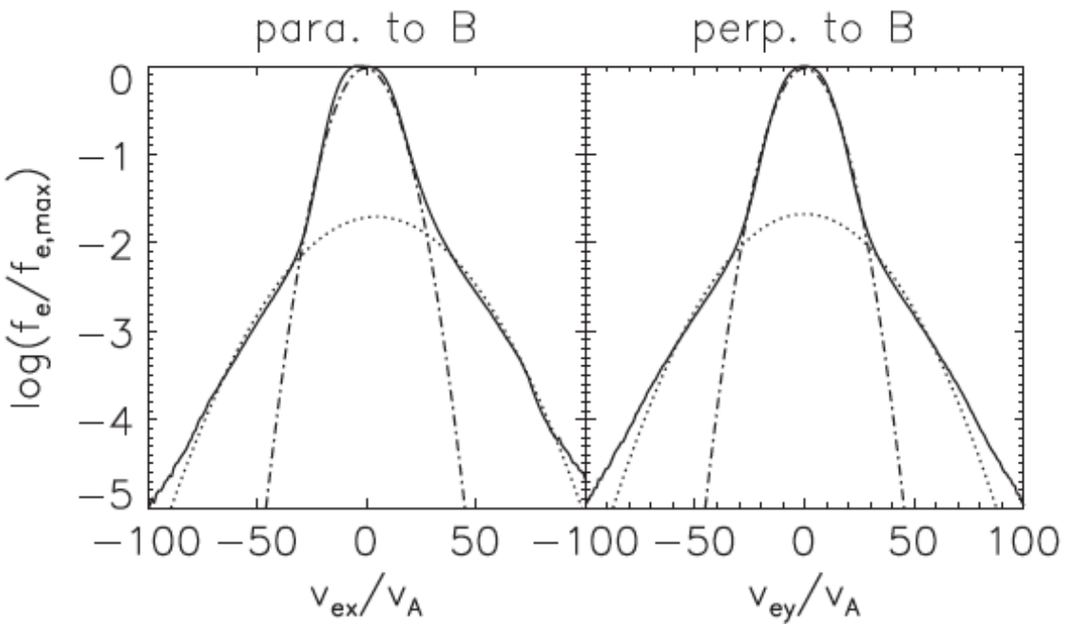

Observation

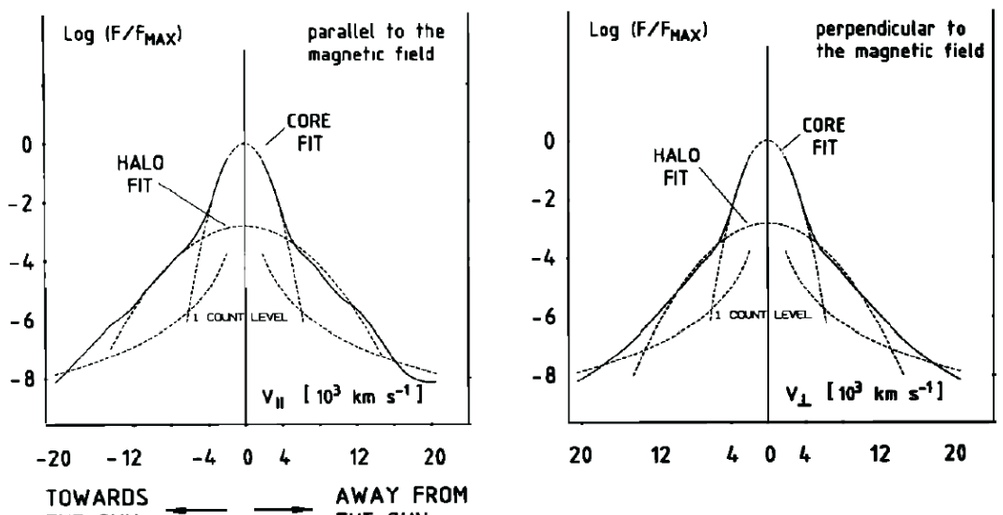

Intrinsic relations between corn-halo:

1: $$\frac{T_{\rm hot}}{T_c} \sim \frac{(1-C_T)}{C_T}\frac{n_c}{n_{\rm hot}} + 4.$$

energy conversion factor from beam kinetic energy into thermal energy, Ct ~ 0.9-1.

$$n_{hot} = n_h + n_s, \quad T_{hot} = (n_h T_h + n_s T_s)/(n_h + n_s)$$

h=halo, s=strahl

2: The mean relative drift between the core and halo-strahl is about the core thermal speed, a relics of electron two-stream instability.

WIND Observation on the Core-Halo-strahl Temperature Relation

$$T_{hot}/T_c \sim 4$$

$$\frac{T_{\rm hot}}{T_c} \sim \frac{(1-C_T)}{C_T}\frac{n_c}{n_{\rm hot}} + 4.$$

O^{7+}/O^{6+} from around 0.002–0.02, we can predict an increase of around 25 % in T_O in the corona. The expected core–halo relationship from Che and Goldstein (2014) shown in Eq. (2) then suggests an increase of 25 % should also appear in $T_{h-s\perp}$, should it be preserved out to 1 AU. The increases in the mean $T_{h-s\perp}$ in these regions in Fig. 7a and b appear to be around 20 %, showing reasonable agreement with the prediction. This implies that there may be an underlying relationship between $T_{h-s\perp}$ and O^{7+}/O^{6+} which for low-O^{7+}/O^{6+} wind has been smeared out in a mostly random fashion, either in the corona itself or by processing in the solar wind.

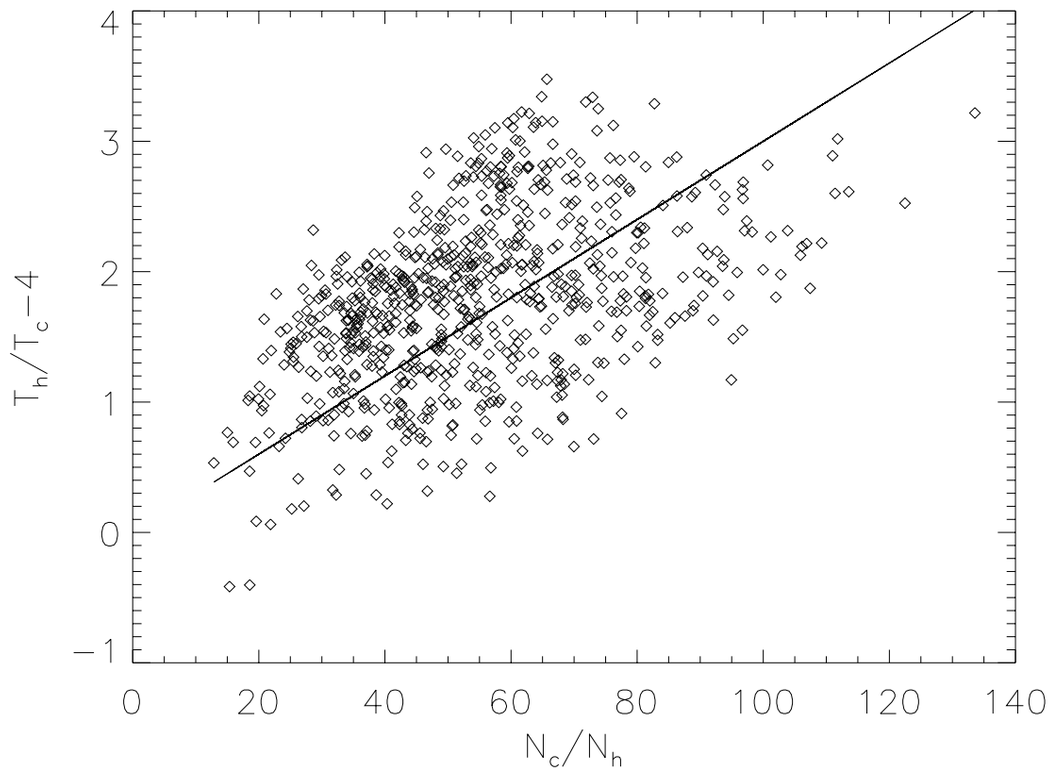

One day Slow Wind data
At solar minimum

Macneil et al, Ann Geophys, 2017

How Electron Beam Density Affects the Formation of Electron Halo?

- We discovered that the electron beam density n_b beyond $0.3n_0$, (n_0 is the background density) the electron halo can not be developed.

- Heating of the core electrons become weaker with decreasing beam density while the heating of halo electrons becomes stronger, explaining the physical meaning of the predicted anti-correlated relation.

$$\frac{T_{\text{hot}}}{T_c} \sim \frac{(1 - C_T)}{C_T} \frac{n_c}{n_{\text{hot}}} + 4.$$

Simulation Initial Parameters

	Run 1	Run 2	Run 3	Run 4	Run 5
δ	0.05	0.1	0.2	0.4	0.5
n_b/n_{c0}	0.053	0.11	0.25	0.67	1.0
v_b	80	60	40	20	15
v_d	84.2	66.6	50.0	33.4	30.0
v_p	24.6	24.6	23.2	0	0
$\gamma/\omega_{pe,0}$	0.29	0.35	0.4	0.38	0.38
$k_f d_i$	13	17	20	30	33
W_D	43.6	54.4	58	43.6	42.5
K	1.68	1.98	2	1.33	1.13

Note. $\delta = n_b/n_0$—ratio of electron beam density to background electron density; n_b/n_{c0}—density ratio of the beam and the core; v_b—beam drift; v_d—relative drift; v_p—the phase speed of ETSI; γ—growth rate; k_f—wave-number of the fastest growing mode; W_D—beam kinetic energy flux; K—the total kinetic energy of the core-beam.

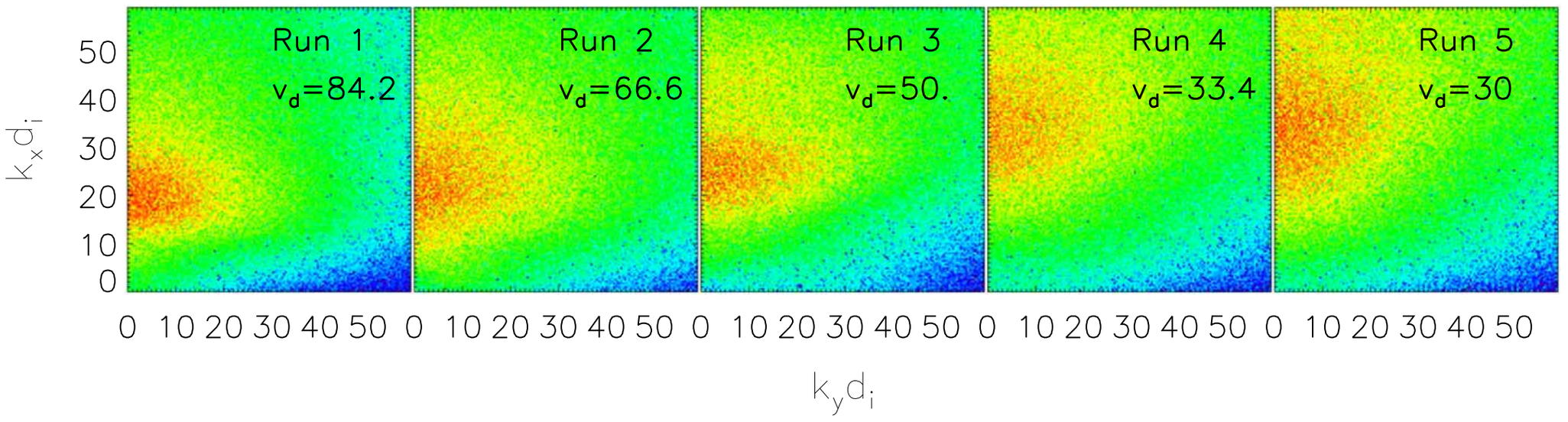

Figure 3. 2D power spectra (in logarithmic scale) of the parallel electric field fluctuation δE_x for different relative drifts.

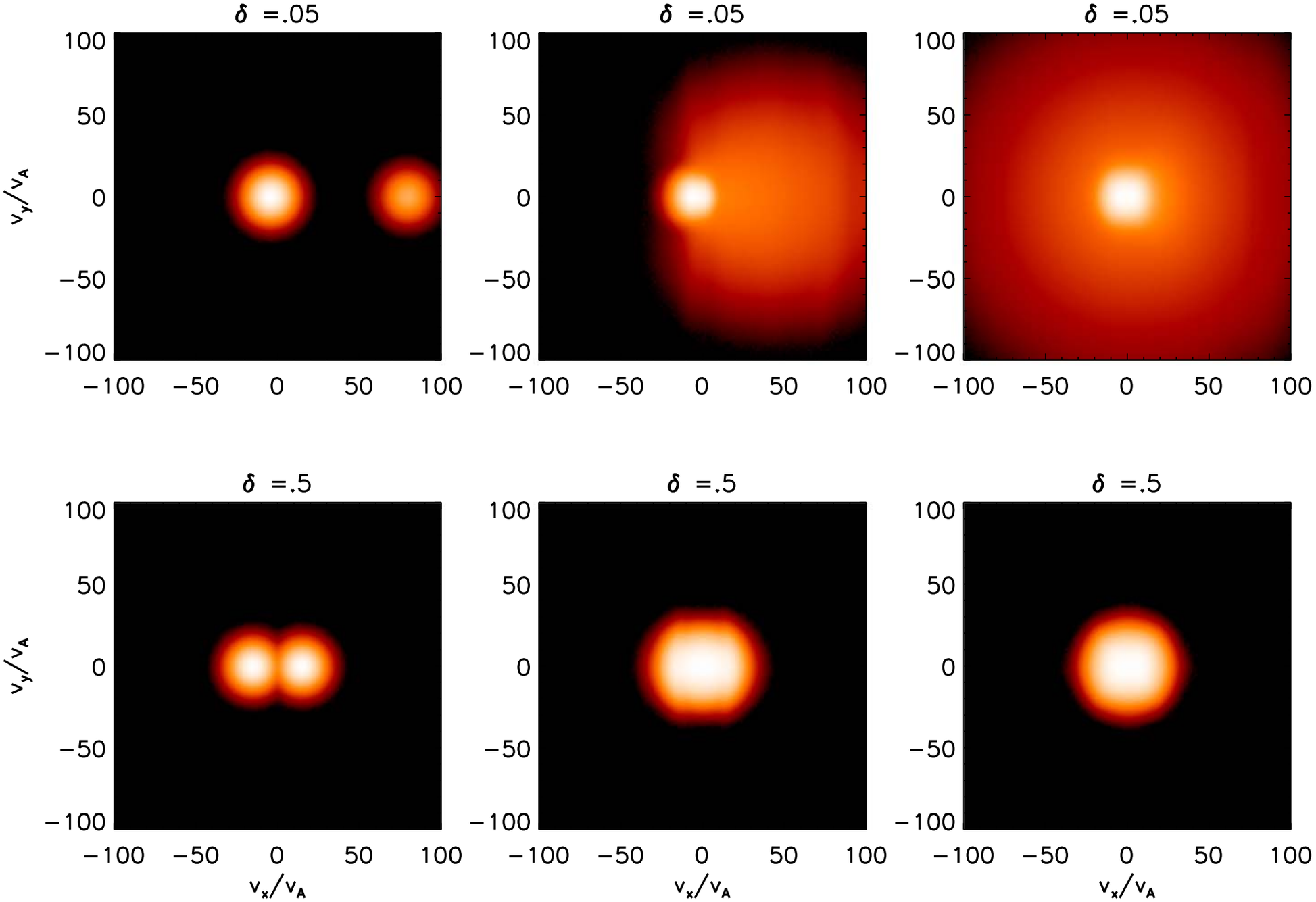

Figure 5. The 2D electron VDFs at different times for Run 1 (upper panels) and 2 (lower panels). Left panel: $\omega_{pi}\, t = 0$; middle panel: $\omega_{pe,0}t = 800$; right panel: $\omega_{pe,0}t = 10{,}400$. A logarithmic scale is used in the plots.

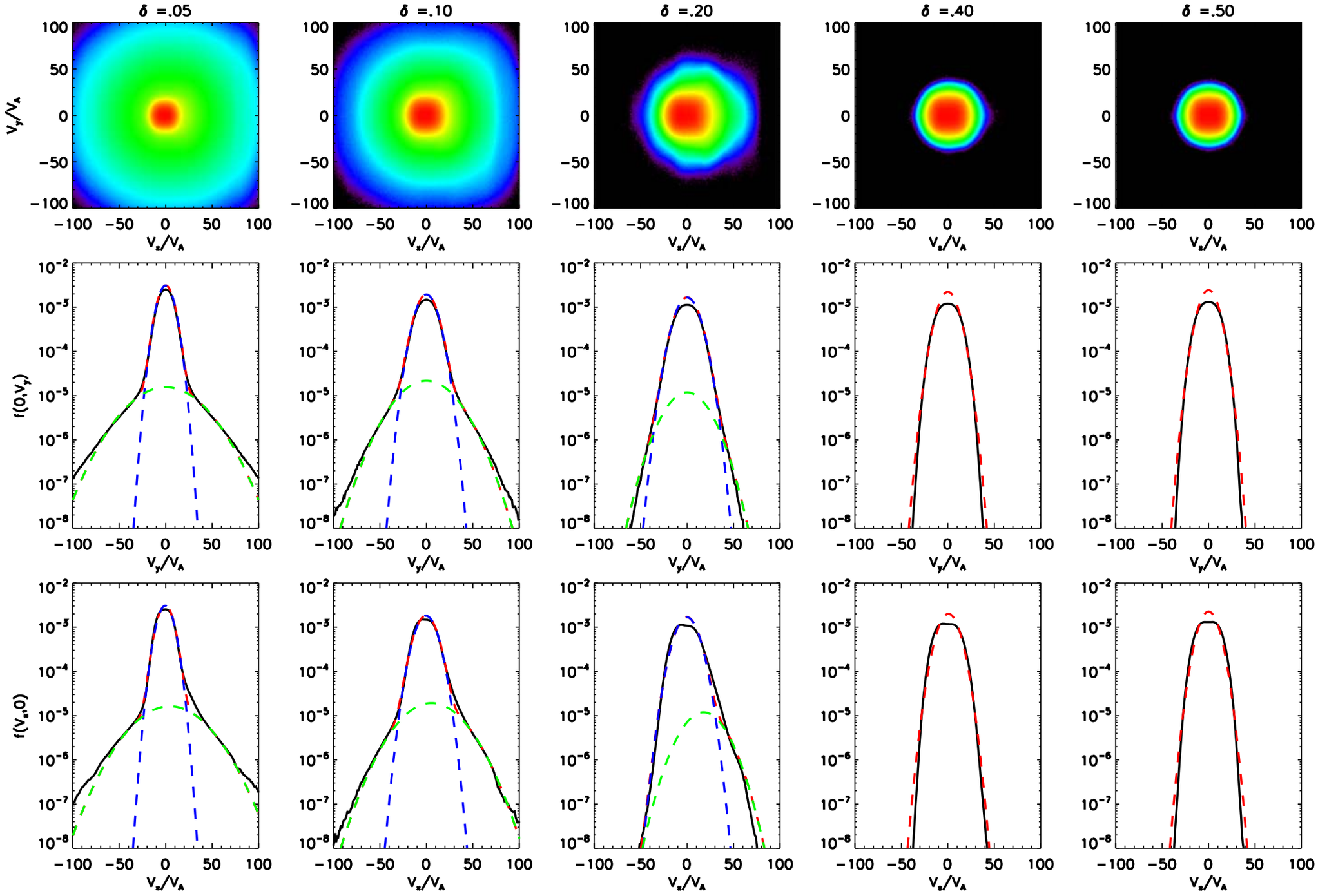

Figure 6. Top panels: images of electron VDFs $f(v_x, v_y)$ in the 2D velocity space (v_x, v_y) at $\omega_{pe,0}t = 10{,}400$. Middle panels: cuts of the 2D electron VDFs along the magnetic field. Bottom panels: cuts of the 2D electron VDFs perpendicular to the magnetic field. The red dashed lines are the total bi-Maxwellian functional fit (a sum of green and blue lines). The model parameters are shown in Table 2.

Conclusions

- We discovered that the electron beam density n_b beyond $0.3n_0$, (n_0 is the background density) the electron halo can not be developed.

- Heating of the core electrons become weaker with decreasing beam density while the heating of halo electrons becomes stronger, explaining the physical meaning of the predicted anti-correlated relation.

$$\frac{T_{\rm hot}}{T_c} \sim \frac{(1-C_T)}{C_T}\frac{n_c}{n_{\rm hot}} + 4.$$